Interface engineered paclitaxel-based hollow mesoporous organosilica nanoplatforms for photothermal-enhanced chemotherapy of tumor

Chunxi Qian[a], Bandar Al-Hamyari[a], Xiaofei Tang[a], Bo Hou[b], Shuaibo Yang[a], Guifang Zhang[a], Huijuan Lv[a],Zhigang Yang[a], Zhaohui Wang[a*], Yanbin Shi[a*]

[a] School of Pharmacy, Lanzhou University, Lanzhou 730030, Gansu, P.R. China

[b] School of Physics and Astronomy, Cardiff University, Cardiff, Wales, CF243AA, United Kingdom

Graphical abstract

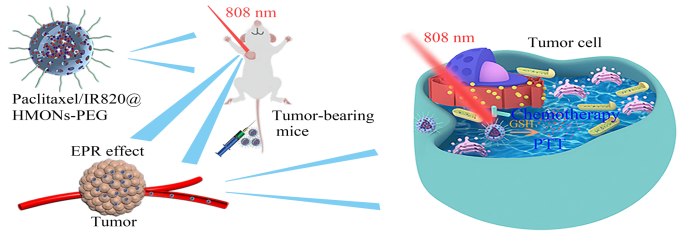

A novel engineered nanosystem based on hollow mesoporous organosilica nanoparticles(denoted as Paclitaxel/IR820@HMONs-PEG) for photothermal-enhanced chemotherapy of tumor.

ABSTRACT

Having benefited from the combination of different therapeutic modalities, functionalized nanoplatforms with synergistic strategies have aroused great interest in anticancer treatment. Herein, an engineered, biodegradable hollow mesoporous organosilica nanoparticles (HMONs) based nanoplatform was fabricated for photothermal-enhanced chemotherapy of tumor. For the first time, we demonstrated that HMONs could serve as nanocarriers for co-delivering of both the paclitaxel and photothermal agent new indocyanine green (IR820) - denoted as Paclitaxel/IR820@ HMONs-PEG. The as-prepared nanosystem exhibited a high paclitaxel-loading capacity of 28.4 %, much higher than those most paclitaxel-loaded nano-formulations. Furthermore, incorporating thioether-bonds (S-S) into the HMONs' framework enabled them with GSH-responsive biodegradation behavior, leading to the controllable release of drugs under tumor reducing microenvironment, and hindered the premature release of paclitaxel. Upon irradiated with NIR laser, the obtained co-delivery nanosystem

* Corresponding author
Email address: wangzhaohui@lzu.edu.cn (Z. Wang.), Tel. 86-931-8915685; Fax. 86-931-8915686.
shiyb@lzu.edu.cn (Y. Shi.), Tel. 86-931-8915685; Fax. 86-931-8915686.

exhibited great photothermal properties generated from IR820. The fabricated nanocomposites could significantly suppress tumor growth under NIR laser irradiation, as validated by *in vitro* and *in vivo* assessments. Combined with outstanding biocompatibility, the constructed nanosystem holds great potential in combinational antitumor therapy.

Keywords: Hollow mesoporous organosilica nanoparticles; Glutathione-responsive biodegradation; Co-delivery; Controlled release; Biocompatibility; Photothermal-enhanced chemotherapy

1. Introduction

So far, cancer remains severe diseases threatening human health[1]. Traditional chemotherapy has shown to be effective in clinical practice. However, it still faces tremendous challenges, such as nonspecific biodistribution, fast metabolism and multidrug resistance (MDR)[2,3]. Considering the inherent shortcomings of traditional chemotherapy, the exploitations and applications of versatile drug delivery systems have flourished [4-6]. For instance, intelligent drug delivery systems are paid considerable attention due to the controllable drug release and reduced systemic toxicity[7-10]. However, numerous studies have also shown that monotherapy is usually insufficient to achieve satisfying therapeutic responses, resulting from the intrinsic heterogeneity and complexity of tumors, which remains a challenge for drug delivery[11-18].

Nanoplatforms integrated with multiple therapeutic agents have provided a new approach for improving antitumor efficiency[19-22]. NIR-laser induced hyperthermia with a combination of chemotherapy can facilitate intracellular drug release and improve chemosensitivity of tumor cells[23-26]. Hollow mesoporous organosilica nanoparticles (HMONs) are molecularly organic-inorganic hybridized frameworks with large cavity space, tunable pore sizes, controllable sizes, good biodegradable and biocompatibility, which are promising for biomedical applications[27-30]. Based on the "chemical homology" mechanism, Huang and co-workers[31] reported the first sub 50 nm HMONs for doxorubicin delivery. Upon exposed to tumor reducing microenvironment, the disulfide bonds incorporated nanoparticles went through fast biodegradation and

accelerated drug release. Huang et al.[32] also reported thioether-bridged hollow mesoporous organosilica nanospheres anchoring with sonosensitizers (protoporphyrin, PpIX) and chelated paramagnetic Mn^{2+} for MRI-guided sonodynamic therapy of tumor. Chen et al.[33] fabricated CuS-modified HMONs encapsulated with perfluoropentane to achieve tri-modal imaging guided bubble-enhanced oxygen-sensitized radiotherapy of cancer. Moreover, Zhang et al.[34] synthesized hybridized deformable mesoporous organosilica nanocapsules (DMONs) incorporated with different organic functional groups through a general and facile way, and successfully applied them for doxorubicin or paclitaxel delivery. Up to now, the development of HMONs-based nanoplatforms is in its fancy age, and the exploration of versatile engineered nanomaterials are still challenging.

Paclitaxel, known as a traditional chemotherapeutic anticancer agent, has widespread use in clinical applications. However, the poor water solubility, nonspecific distribution, rapid degradation, and multidrug resistance remain great challenges in the clinic[35-37]. The researchers have developed versatile drug delivery systems to solve these problems, while most paclitaxel-based nano-formulations suffered from low loading capacity and premature release of paclitaxel, which results in large injection doses and inevitable systemic side effects[38-40].

Benefit from the advantages of HMONs, they were adopted to improve the loading capacity of paclitaxel and endow them with GSH-triggered drug release behavior. Considering the high efficiency of synergistic therapy, a novel nanosystem based on paclitaxel and IR820 co-loaded HMONs (Paclitaxel/IR820@HMONs-PEG) has been successfully constructed for combinational chemo-photothermal therapy of tumor (Scheme 1). HMONs with particle size around 90 nm were constructed via a “chemical homology” approach, and the functionalization of disulfide bonds enabled them with GSH-responsive biodegradation behavior. Comprehensive *in vitro* analysis including glutathione-responsive drug release behavior, photothermal effects, and biocompatibility evaluation of synthesized nanosystems were investigated. Furthermore, both *in vitro* and *in vivo* tumor inhibition assessments were performed to analyze the combinational antitumor effects.

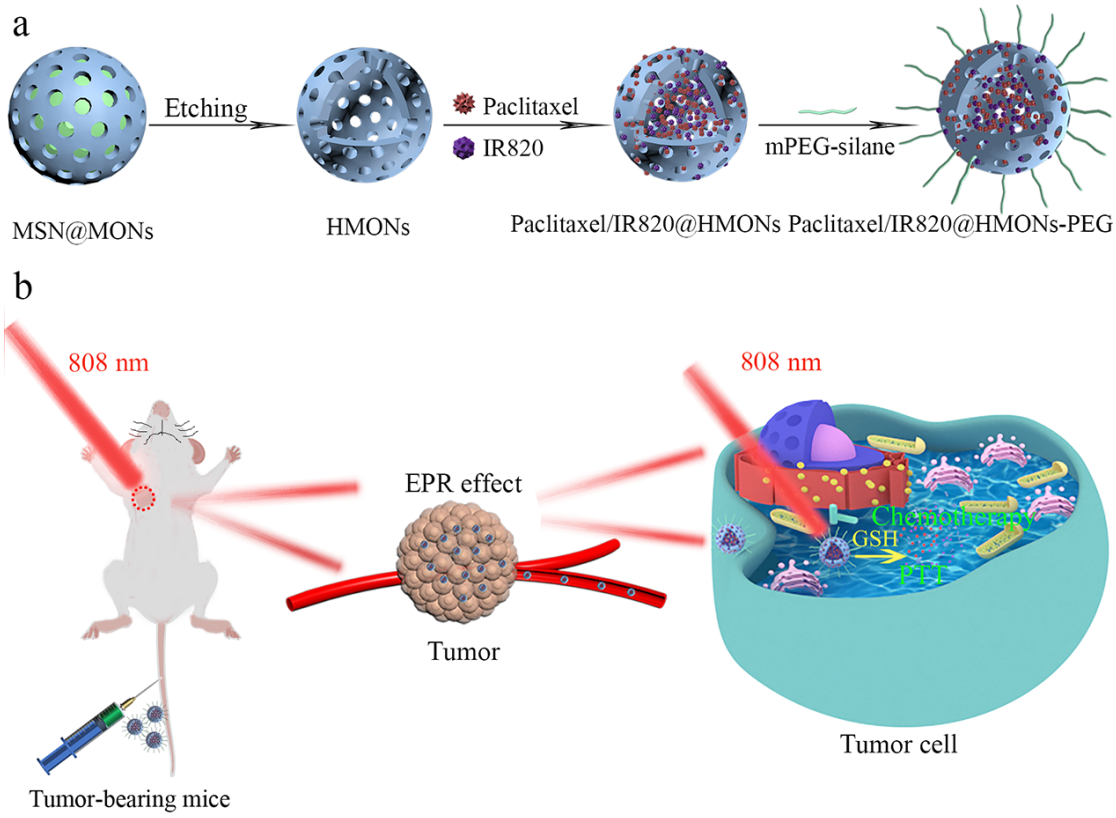

Scheme 1. Schematic illustration of a) the synthesis of Paclitaxel/IR820@HMONs-PEG nanoparticles; and b) the mechanism of Paclitaxel/IR820@HMONs-PEG nanoplatform for synergistic chemo-photo-thermal antitumor therapy.

2. Materials and methods

2.1 Materials

Cetyltrimethylammonium chloride (CTAC), tetraethyl orthosilicate (TEOS), triethanolamine (TEA), ammonia solution (25-28 %), mPEG-silane (PEG, Mw: 2000 Da) , glutathione (Reduced) and tween-80 (Polysorbate) were provided by Aladdin Biochemical technology Co. (Shanghai, China). Bis(triethoxysilylpropyl) disulfide (BTDS) and new indocyanine green (IR820) were sourced from Macklin Biochemical Co. (Shanghai, China). Paclitaxel was supplied by Energy Chemical Co. (Shanghai, China). Ethanol, concentrated hydrochloric acid (HCl, 37 %) were purchased from Sinopharm Chemical Reagent Co. (Shanghai, China). 4T1 cells were provided by Procell Biotech Co. (Wuhan, China). RPMI 1640, fetal bovine serum (FBS), phosphate-buffered saline (PBS), 1% penicillin-streptomycin and 0.05% trypsin-EDTA were supplied by Excell Biotechnology (Shanghai, China). 4', 6-diamino-2-phenylindole (DAPI) and calcein AM/PI assay kit were provided by Beyotime Biotechnology

(Shanghai, China). Cell counting kit-8 (CCK-8), annexin V-FITC/PI assay kit, and TUNEL apoptosis detection kit (Alexa Fluor 488) were received from Yeasen Biotech Co. (Shanghai, China). Deionized (DI) water of 18.25 MΩ was employed in experiments. All reagents were used as received.

2.2 Characterization

The nanoparticles′ morphology were observed using Tecnai F30 transmission electron microscope (FEI Company, Hillsboro, USA) with accelerating voltage of 200 KV. Nitrogen (N_2) adsorption-desorption instrument (Micromeritics, Norcross, USA) was applied to detect the specific surface area and pore size distribution of the nanoparticles. The hydrodynamic diameter and zeta potential were obtained from Nano ZS90 Zetasizer instruments (Malvern Panalytical, Malvern, UK). Organic molecular spectroscopies were obtained using Nicolet 6700 Fourier infrared spectrometer (FTIR, Thermo Fisher Scientific, Waltham, USA) and UV-3600 spectrometer (UV-vis-NIR, Shimaduz, Tokyo, Japan). Raman spectroscopy was taken on WITec alpha 300 R confocal Raman spectroscopy (WITec, German). FV1000 CLSM (Olympus, Tokyo, Japan) was applied to study the cellular uptake behavior. BD LSRFortessa flow cytometer was used for cell apoptosis analysis (Becton Dickinson, Franklin Lakes, USA). Photothermal properties were studied by 808 nm NIR laser (Changchun Institute of Optics, Fine Mechanics and Physics, Chinese Academy of China, Changchun, China) and GTC 400 C infrared thermal camera (Robert Bosch Tool Corporation, Germany). FVISQUE InVivo Smart *in vivo* imaging system (Viework, Korea) was employed to observe the nanoparticles' biodistribution in mice.

2.3 Synthesis of thioether-bridged HMONs

HMONs were prepared based on the previous reported ammonia-assisted selective etching method[41].

2.4 Fabrication of paclitaxel/IR820@HMONs-PEG

HMONs (50 mg) was dispersed into ethanol (25 mL) under ultrasound sonication. Then, 5 mL of DMSO solution containing pre-dissolved 25 mg of paclitaxel and 25 mg of IR820 was swiftly mixed with the HMONs dispersion. After reacting in the darkroom for 24 h, 20 mg of mPEG-silane was added and reacted for another 4 h. The reaction

mixture was dialyzed against DI water (cellulose membrane, cutoff Mw: 5000 Da) for 48 h. The final products (designated as Paclitaxel/ IR820@ HMONs-PEG) were stored under 4 ℃ for future use.

The loading capacity and encapsulation efficiency of paclitaxel were evaluated (at λ_{227} nm) by HPLC (Agilent 1260, Agilent Technologies Inc, USA). The eluent were methanol and water (75:25, v/v), and the flow rate was 1.0 mL/min. In addition, the IR820 loading capacity and encapsulation efficiency were measured using UV-Vis-NIR absorption spectrometer at λ_{690} nm.

2.5 *In vitro* glutathione-responsive drug release behavior and photothermal effects

5 mg of Paclitaxel/IR820@HMONs-PEG nanoparticles was encapsulated in dialysis bags (cutoff Mw: 5000 Da), immersing in PBS solution (pH 7.4, 30 mL) containing 20% tween-80 at GSH concentrations of 0, 5, 10 mM. They were then placed into the shaking table at 100 rpm under 37 ℃ for 48 h. The GSH-triggered drug release of paclitaxel and IR820 was evaluated at specific time intervals.

To evaluate the photothermal performance, Paclitaxel/IR820@HMONs-PEG suspensions at various concentrations (0, 50, 100, 200, 250 μg/mL) were separately receiving 808 nm laser irradiation (1 W/cm^2, 10 min). Afterwards, the nanocomposites (100 μg/mL) were illuminated with NIR-laser under power densities of 0.5, 0.75, 1.0, 1.2, 1.5 W/cm^2, respectively. Five repetitive laser on/off cycles were performed to analyze the photothermal stability of the nanocomposites (100 μg/mL). The temperature changes of the samples were measured every 10 seconds with a thermal infrared imaging camera.

2.6 *In vitro* biocompatibility evaluation

Hemolysis tests and *in vitro* cytotoxicity analysis were conducted to testify the biocompatibility of blank HMONs. For hemolysis test, 2 mL of rabbit anticoagulant blood samples was washed with 0.9 % NaCl until the supernatant was transparent. The red blood cells (RBCs) were recovered by centrifugation (3000 rpm, 5 min) and diluted with 0.9 % NaCl (100 mL). RBCs suspensions (2 mL) were mixed with HMONs or HMONs-PEG nanoparticles (2 mL) at concentrations of 50, 100, 200, 400, 600, 800, 1000 μg/mL, respectively, and incubated under 37℃ water bath for 2 h. Deionized

water was the positive control, and physiological saline was the negative control. After centrifugation (3000 rpm, 10 min), the supernatant absorbance was measured by UV-Vis-NIR (λ_{540nm}). The hemolysis ratio was calculated as follows[42].

Hemolysis percent (%) = $[(A_{sample\text{-}RBCs+} - A_{sample\text{-}RBCs-}) - A_{negative}] / (A_{positive} - A_{negative})$.

In vitro cell viability experiments were further performed to analyze the cytotoxicity. Briefly, 4T1 cells were seeded at a density of 5×10^3 cells/well in 96-well plates containing RPMI 1640 (100 μL), containing 10 % FBS and 1 % v/v penicillin – streptomycin. The cells were incubated overnight under humidified atmosphere. The medium was replaced with HMONs or HMONs-PEG (100 μL) at concentrations of 0, 20, 50, 100, 200 μg/mL, respectively. The supernatant was then replaced by 10% CCK-8 solution (100 μL) after 24 h incubation. After another 4 h incubation, the absorbance was detected using microplate reader (Tecan spark, Tecan, Switzerland) at λ_{450nm}.

2.7 Cellular uptake behavior *in vitro*

Flow cytometry (FCM) and confocal laser scanning microscope (CLSM) were applied for characterizing the cellular uptake of cells. 4T1 cells were cultured overnight (5×10^5 cells/well) under humidified atmosphere for CLSM analysis. The medium was replaced by Paclitaxel/IR820@ HMONs-PEG suspensions and incubated for additional few hours (4 or 8 h). After incubated for 2 h, the cells were exposed to 808 nm laser irradiated (1.0 W/cm^2, 5 min) for NIR treatment. After that, the cells were washed and fixed with 4% paraformaldehyde (30 min). Then, the nuclei were marked by DAPI at room temperature, and the cells were washed before CLSM imaging. Furthermore, the intracellular IR820 fluorescence was quantified by flow cytometry. The cells received same treatments as in CLSM experiments. Afterwards, the cells were collected by trypsin-EDTA digestion, resuspend with cold PBS, followed by measured on FCM.

2.8 Cytotoxicity assessments *in vitro*

Since paclitaxel has great therapeutic effects towards breast cancer, 4T1 cells (murine mammary cancer cell line) were adopted to evaluate nanocomposites' cytotoxicity by standard CCK-8 assessments. Typically, 4T1 cells (5×10^3 cells/well) were seeded in 96-well plates under the humidified incubator (37 ℃, 5 % CO_2). The supernatant was then replaced by RPMI 1640 containing paclitaxel, Paclitaxel@HMONs-PEG, free

IR820, IR820@HMONs-PEG and Paclitaxel/IR820@HMONs-PEG nanoparticles at 6.4 μg/mL of paclitaxel and 25 μg/mL of IR820, respectively. For groups treated with NIR irradiation, the cells received 808 nm illumination after 2 h incubation (1 W/cm^2, 5 min). The standard CCK-8 experiments were performed as in Section 2.6 after 24 h incubation. Furthermore, the nanoparticles at various concentrations of paclitaxel were added to testify the dose-dependent cytotoxicity of chemotherapeutic agents (0, 0.8, 1.6, 3.2, 6.4, 12.8 μg/mL). After 24 h incubation, the relative cell viabilities were analyzed *via* CCK-8 kit.

2.9 Live and dead cells observation

For live and dead cells observation, 4T1 cells were cultivated overnight in multiple-well plates (12 wells) under humidified atmosphere. The cells were treated with paclitaxel, Paclitaxel@HMONs-PEG, free IR820, IR820@HMONs-PEG, Paclitaxel/ IR820@HMONs-PEG at 6.4 μg/mL of paclitaxel and 25 μg/mL of IR820 for 12 h, respectively. For cells receiving synergistic treatment, they were exposed to 808 nm laser irradiation (1 W/cm^2, 5 min) after incubated for 2 h. After removing the culture medium, a mixed working fluid of calcein AM (λ_{ex}=490 nm, λ_{em}=515 nm) and PI (λ_{ex}=535 nm, λ_{em}=617 nm) was added to cell suspensions and incubated in a humidified incubator (30 min). After removing the staining solutions, the live (green-labelled by calcein-AM) and dead cells (red-labelled by PI) were visualized using inverted fluorescence microscope (VERT1, Zeiss, USA).

2.10 Cell apoptosis analysis

To quantitatively analyze cell apoptosis, 4T1 cells were cultured in 6-wells plates (5×10^5 cells/well) overnight under humidified atmosphere. The cells were treated as mentioned in Section 2.9. After incubation for 12 h, the cells were digested and washed with cold PBS. Then, a binding buffer (100 μL) was added to resuspend the cells, followed by adding 5 μL of Annexin V-FITC and 10 μL of PI. After another 15 min incubation in the darkroom, 400 μL of the binding buffer was added, and the obtained cell suspensions were immediately measured using flow cytometry.

2.11 *In vivo* biodistribution assessments

Female BALB/c mice (18 - 22 g) were obtained from Lanzhou Veterinary Research

Institute, Chinese Academy of Agricultural Sciences (Lanzhou, China). All the animal experiments were performed following the guidelines of the Animal Care and Use Committee of Laboratory Animal Science, Lanzhou University. To build the tumor-bearing mice model, 4 T1 cells (5×10^6/mouse, 100 μL) were subcutaneously implanted into the left armpit of mice. For *in vivo* biodistribution analysis, two groups (n=3) of randomly assigned tumor-bearing mice were administered with IR820-based nanoparticles (100 μL, 10 mg/kg) *via* intravenous injection. VISQUE In Vivo Smart *in vivo* imaging system was applied for recording the fluorescence intensity of the mice at predetermined time intervals.

2.12 Tumor inhibition experiments *in vivo*

The *in vivo* antitumor performance of Paclitaxel/IR820@HMONs-PEG was investigated by preparing tumor-bearing mice in according to the procedures as depicted in Section 2.11. When tumor volumes grew up to approximately 100 mm^3, seven groups (n=5) of randomly divided mice were treated with (i) PBS+NIR, (ii) paclitaxel, (iii) Paclitaxel@HMONs-PEG, (iv) free IR820+NIR, (v) IR820@HMONs-PEG+NIR, (vi) Paclitaxel/IR820@ HMONs-PEG, (vii) Paclitaxel/IR820@HMONs-PEG+NIR (Paclitaxel: 5mg/kg, IR820: 10 mg/kg). The mice were intravenously injected 200 μL of different nanoparticles on the 3^{rd}, 6^{th}, 9^{th}, 12^{th} day through the 21-day treatment process. NIR laser irradiation (1W/cm^2, 10 min) was applied on the mice receiving synergistic treatment after 8 h post-injection. Meanwhile, the infrared thermal camera was employed to record the temperature changes of the tumor sites. The relative body weights and tumor sizes were measured every 3 days. The tumor volumes were calculated as $V=L\times W^2/2$, where L represented the length of tumor and W indicated the width of tumor.

2.13 Histopathological examination

The tumors were harvested from mice after the treatment to further estimate the therapeutic effect, and paraffin sections were made for histological assessments, including H&E staining and TUNEL staining. Heart, kidney, liver, lung, spleen were prepared for H&E analysis. The mice were sacrificed after 21-day treatment, and major organs were harvested to analyze the histological changes *via* H&E staining. For

hematology and blood chemistry tests, 12 healthy mice were treated with free paclitaxel and paclitaxel-loaded nanoparticles (200 μL, Paclitaxel: 5 mg/kg). After 21 days, blood (0.5 mL each) from all sacrificed mice were taken out for analysis.

2.14 Statistical analysis

All results were presented as mean ± standard deviation, and one-way ANOVA analysis accompanied by the post hoc Tukey's test was applied for statistics with statistical significance assigned at $*P < 0.05$ (significance), $**P < 0.01$ (moderate significance), $***P < 0.001$ (high significance).

3. Results and discussion

3.1 Synthesis and characterization of Paclitaxel/IR820@HMONs-PEG

The as-prepared HMONs are dispersed (average size of 90 nm) with worm-like mesoporous channels homogeneously distributed within the framework (Figure 1a). As shown in Figure 1b, after loaded with therapeutic agents and surface modification, the internal void space and mesoporous channels of HMONs almost disappear, confirming the successful nanocomposite fabrication. Elemental mapping images indicate that C, Si, O and S uniformly distribute in the framework of HMONs (Figure 1c-h). Energy dispersive X-ray (EDX) spectrum also verifies the existence of C, Si, O and S in the skeleton (Figure. S1). N_2 adsorption and desorption isotherms show mesoporous structure with surface area of 419.7 m^2g^{-1} and uniform pore size of 5.2 nm (Figure. 1i-j). As shown in Figure 1k, the distinct stretching vibrations extract from Raman spectroscopy at 487 cm^{-1} and 500 cm^{-1} are related to disulfide bonds (-S-S-), and the peak of 634 cm^{-1} indicates the presence of -C-S- in the structure[43,44].

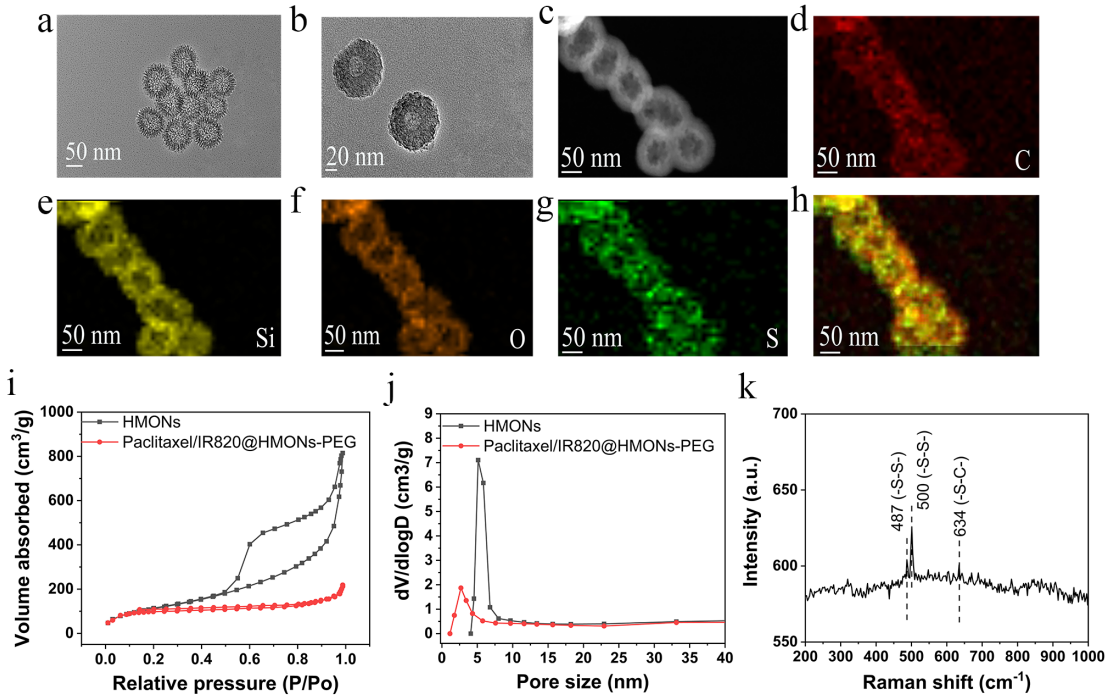

Figure 1. Structural and compositional characterization of HMONs and Paclitaxel/IR820@HMONs-PEG.Transmission electron microscopy (TEM) images of a) HMONs, b) Paclitaxel/IR820@HMONs-PEG. c)Acquired HAADF scanning and corresponding area-elemental mappings of HMONs: d) C, e) Si, f) O, g) S, and h) merged images.Scale bar: 50 nm. i)N_2 adsorption-desorption isotherm and j)pore size distribution spectra of HMONs and Paclitaxel/IR820@HMONs-PEG.k)Raman spectra of HMONs.

The hydrodynamic size of HMONs increases from 113.5 ± 2.18 nm to 125.3 ± 9.15 nm as a function of synthetic steps (Figure. 2a). The zeta potential of HMONs varies from -25.3 ± 1.27 mV to -29.4 ± 1.14 mV (Figure. 2b). The above results confirmed that the surface modifications were achieved. The absorption peaks at 227 nm and 820 nm of Paclitaxel/IR820@HMONs-PEG are revealed from the UV-Vis-NIR absorption spectroscopy (Figure. 2c), indicating the successful encapsulation of paclitaxel and IR820. The FT-IR spectrum displays the characteristic absorption peaks of paclitaxel (3440 cm^{-1} of -OH, 1713 cm^{-1} and 1734 cm^{-1} of -C=O-, 1646 cm^{-1} of -C=N-) and IR820 (1500cm^{-1} and 1600 cm^{-1} of -C_6H_5, 1330 cm^{-1} and 1140 cm^{-1} of -O=S=O-), respectively, confirming the successful loading of the therapeutic agents (Figure. 2d). Meanwhile, the encapsulation efficiency was calculated to be 79.3 % of paclitaxel and 90.7 % of IR820, and the relevant loading capacity was measured to be 28.4 % and 31.2 %. The loading capacity of paclitaxel was much higher than those most reported paclitaxel-loaded nanoystem, deriving from the enhanced hydrophobic interactions between paclitaxel and organosilica bridged framework, which is beneficial to achieve desirable therapeutic effects with small amounts of nanocomposites. Dynamic light scattering

analysis reveals that the prepared nanocomposites can be well dispersed in DI water, saline, PBS, culture medium, culture medium + 10 % FBS, with average hydrodynamic diameters of 125.3 ± 9.15 nm, 127.3 ± 8.28 nm, 127.8 ± 2.59 nm, 129.9 ± 5.66 nm, 134.5 ± 5.16 nm, respectively, as shown in Figure S2. The dispersions show no apparent agglomeration or size variation within 72 h, indicating the prepared nanocomposites have good colloidal stability in these physiological medium.

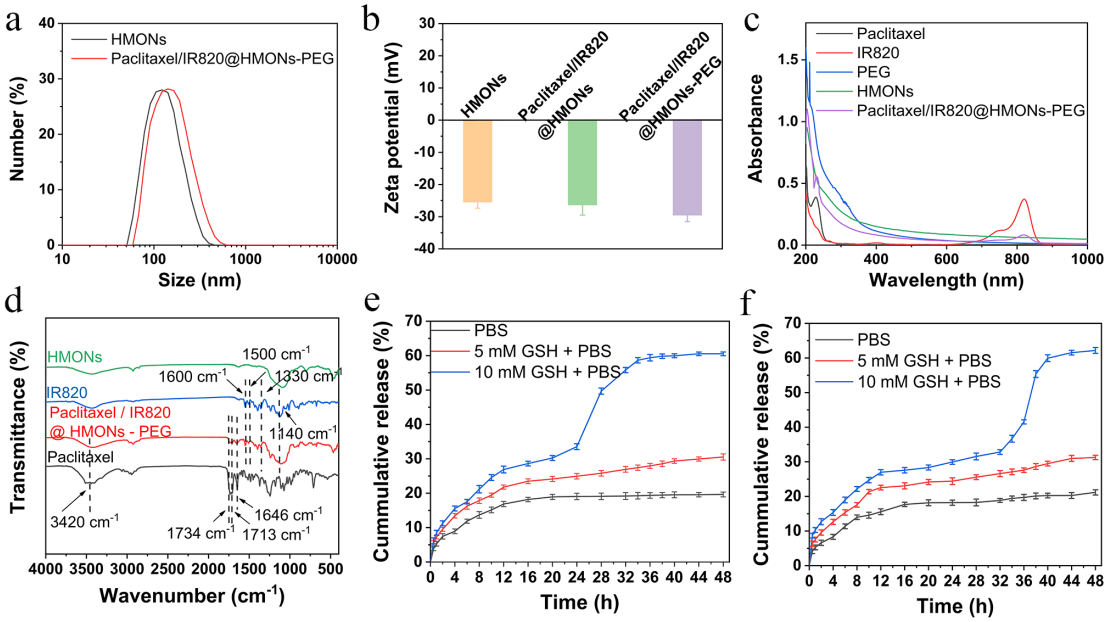

Figure 2. Characterization data on the fabricated nanoparticles. (a) Hydrodynamic size of HMONs and Paclitaxel/IR820@HMONs-PEG nanoparticles.(b)The zeta potentials of HMONs, Paclitaxel/IR820@HMONs and Paclitaxel/IR820@HMONs-PEG.(c)UV-Vis-NIR spectrum of paclitaxel, IR820, PEG, HMONs and Paclitaxel/IR820@HMONs-PEG.(d)FT-IR spectrum of paclitaxel, IR820, HMONs, and Paclitaxel/IR820@HMONs-PEG. *In vitro* (e) paclitaxel and (f) IR820 cumulative release profiles of Paclitaxel/IR820@HMONs-PEG at different GSH concentrations.

3.2 GSH-responsive drug release

It has been reported that disulfide bonds introduced into the HMONs' framework were easily broken in the tumor reducing environment, further leading to controlled drug release and enhanced therapeutic effects[45]. Thus, the release behavior of paclitaxel and IR820 was evaluated under different GSH concentrations at the predetermined time. As shown in Figure 2e-f, when the nanocomposites were kept in 10 mM GSH after 24 h, the disulfide bonds imbedded in the HMONs' framework were largely broken, contributing to large-scale degradation of the nanocarriers. After 48 h, the amounts of released paclitaxel and IR820 are only 19.6 % and 21.1 % in PBS, which indicates that the fabricated nanocomposites have great stability under physiological environment. However, the release rates of paclitaxel and IR820

gradually increase to 30.5 % and 31.2 % when exposed to 5 mM GSH within 48 h, which can be explained by the slow biodegradation of HMONs under mild reducing medium. The drug release amount of both paclitaxel and IR820 drastically increased to 62.5% and 65.2 % under 10 mM GSH in 48 h. However, compared with traditional organic nanocarriers, the degradation rate of HMONs is still relatively low. The level of GSH (10 mM) is similar to that in the tumor microenvironment[46-48]. The accelerated drug release indicated the distinctive cleavage of disulfide bonds of the framework and subsequent fast biodegradation of HMONs. The GSH-dependent drug release behavior could ensure tumor specific drug delivery and minimize the amount of premature drug release during blood circulation.

3.3 Photothermal performance

The photothermal properties of Paclitaxel/IR820@HMONs-PEG were also studied. As depicted in Figure 3a-c, the synthesized nanomaterials display strong photothermal effects, showing concentration and power density-dependent temperature rising behavior. In addition, there are no significant temperature changes observed under five on/off cycles irradiation, showing that the fabricated nanoparticles have great photothermal stability (Figure 3d).

3.4 *In vitro* biocompatibility

Typically, hemolysis tests and cytotoxicity assessments were performed to analyze the biocompatibility of blank nanoparticles. However, no obvious hemolysis is observed among series concentrations of nanoparticles, even at 1000 μg/mL of HMONs or HMON-PEG, as measured by UV-Vis-NIR spectrometer (Figure 3e), which might be attributed to the reason that the as-introduced organic group significantly reduced the number of -OH in the framework[49]. Moreover, the cell viabilities are kept above 90% even when treatment with HMONs or HMONs-PEG (250 μg/mL) under 24 h incubation (Figure 3f). These results demonstrated that the blank nanoparticles were of great biocompatibility, which was beneficial for biological application.

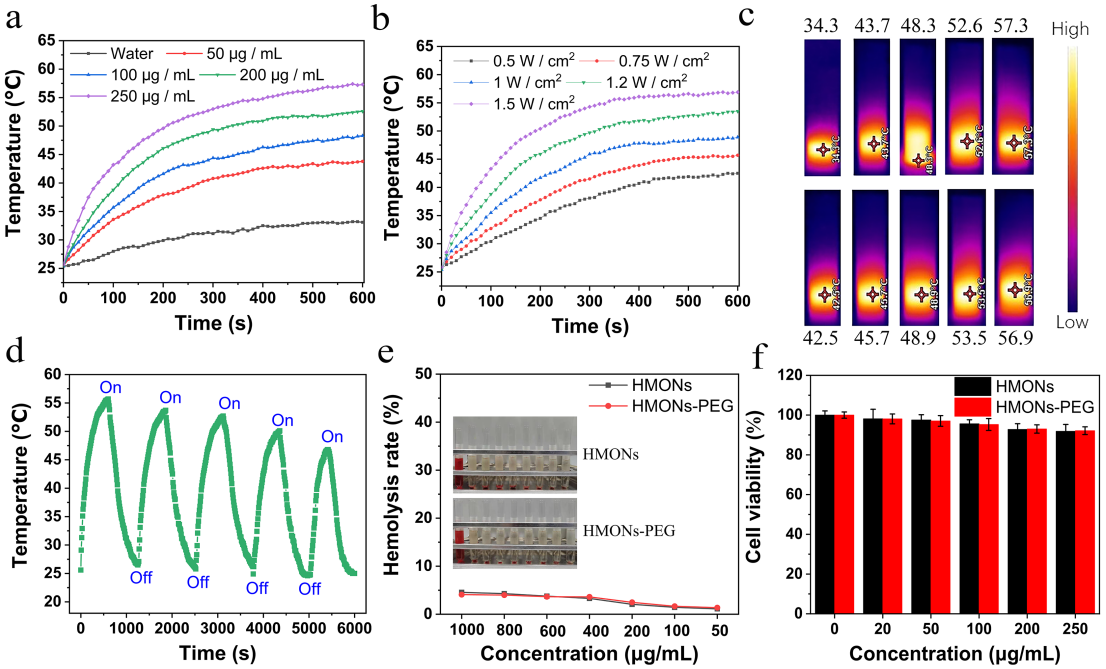

Figure 3.Temperature increase profiles of Paclitaxel/IR820@HMONs-PEG suspensions at different concentrations (a) and power densities (b)upon 808nm laser irradiation(1.0 W/cm^2,10 min).(c)Photothermal images of Paclitaxel/IR820@HMONs-PEG after NIR irradiation for 10 min,with different nanoparticle concentrations(top) and power densities (bottom).(d)Photothermal stability of Paclitaxel/IR820@HMONs-PEG under five on/off cycles of laser irradiation.(e)Hemolytic percentage of RBCs after incubated with HMONs or HMONs-PEG suspensions for 2 h.Insert:photographs of the corresponding hemolysis results of HMONs (top) and HMONs-PEG (bottom). (f)Relative 4T1 cell viability after incubated with HMONs or HMONs-PEG suspensions for 24 h.

3.5 Uptake behavior of 4T1 cells

The intracellular fluorescence of IR820 become stronger with prolonged incubation durations *via* CLSM observation. Under 5 min laser irradiation, the fluorescence of IR820 in the cytoplasm is much more intensive after 8 h incubation (Figure 4a), indicating the enhanced endocytosis of Paclitaxel/IR820@HMONs-PEG attributed to NIR induced mild hyperthermia. The enhanced cellular uptake under laser irradiation is further confirmed by the flow cytometry assessments (Figure 4b-c). Such NIR-improved cellular uptake phenomenon might be derived from the disruptions of the cell membrane, and accelerated drug release behavior induced by mild hyperthermia[50,51].

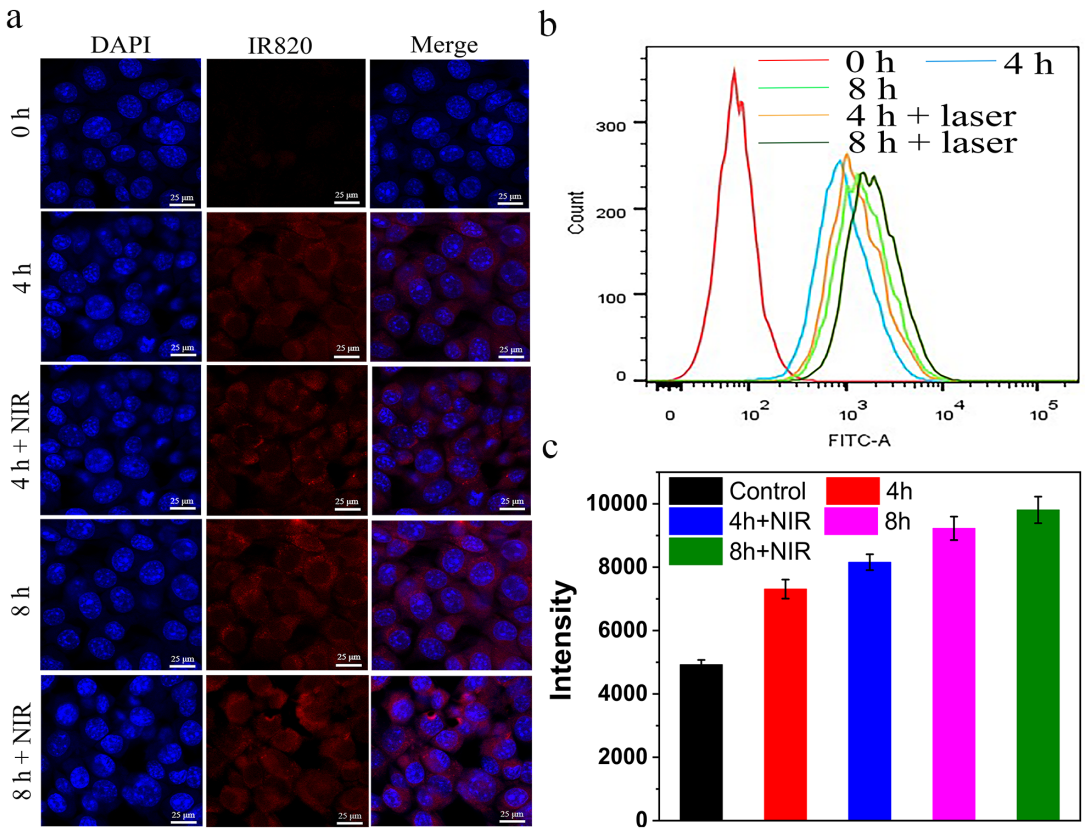

Figure 4. (a) Confocal fluorescence images of 4T1 cells treated with Paclitaxel/IR820 @ HMONs-PEG nanoparticles with or without NIR laser irradiation for different times.Scale bar: 50 μm.(b)Flow cytometry analysis of intracellular fluorescence of Paclitaxel/IR820@ HMONs-PEG and (c) quantitative mean fluorescence intensities after the treatment.

3.6 *In vitro* synergistic chemo-phototherapy

The *in vitro* combinatorial chemo-phototherapy of Paclitaxel/IR820@HMONs-PEG was investigated *via* CCK-8 experiments. The relative cell viabilities are kept above 95 % after PBS treatment regardless of NIR irradiation, while they decrease to 68.33 % after treatment with IR820@HMONs under laser irradiation (Figure 5a), indicating that IR820@HMONs possessed certain efficiency of photothermal therapy. Simultaneously, the cytotoxicity of mono-chemotherapy was also investigated. The cell viabilities are separately 55.67 % and 48.22 % for free paclitaxel and Paclitaxel/IR820@HMONs-PEG. However, the cell mortalities for Paclitaxel/IR820@HMONs-PEG plus laser irradiation are significantly increased to 72.57 %, further confirming the great tumor inhibition effect of photothermal-enhanced chemotherapy. Additionally, the cell viabilities largely decrease with the increasing concentration of paclitaxel (Figure 5b), suggesting the concentration-dependent cytotoxicity of fabricated nanosystem.

To visually observe the therapeutic effects of synthesized nanoparticles, calcein AM/propidium iodide (PI) fluorescent dyes were applied for cell staining. Cell viabilities are not affected in the control group regardless of NIR irradiation, as observed by strong green fluorescence representing live cells. However, as shown in Figure 5c, many 4T1 cells exhibit largely reduced survival after treated with Paclitaxel/IR820@HMONs-PEG under laser irradiation, as indicated by the most intensive red fluorescence representing dead cells. Meanwhile, cell apoptosis is further quantified by flow cytometry analysis. Cells receiving Paclitaxel/IR820@HMONs-PEG+NIR treatment show a larger degree of apoptosis up to 60.46 % compared with 42.35 % of free paclitaxel, while fewer apoptosis or necrosis can be found in other groups (Figure 5d). These results demonstrated that the fabricated nanocomposites possessed efficient chemo-photothermal antitumor properties.

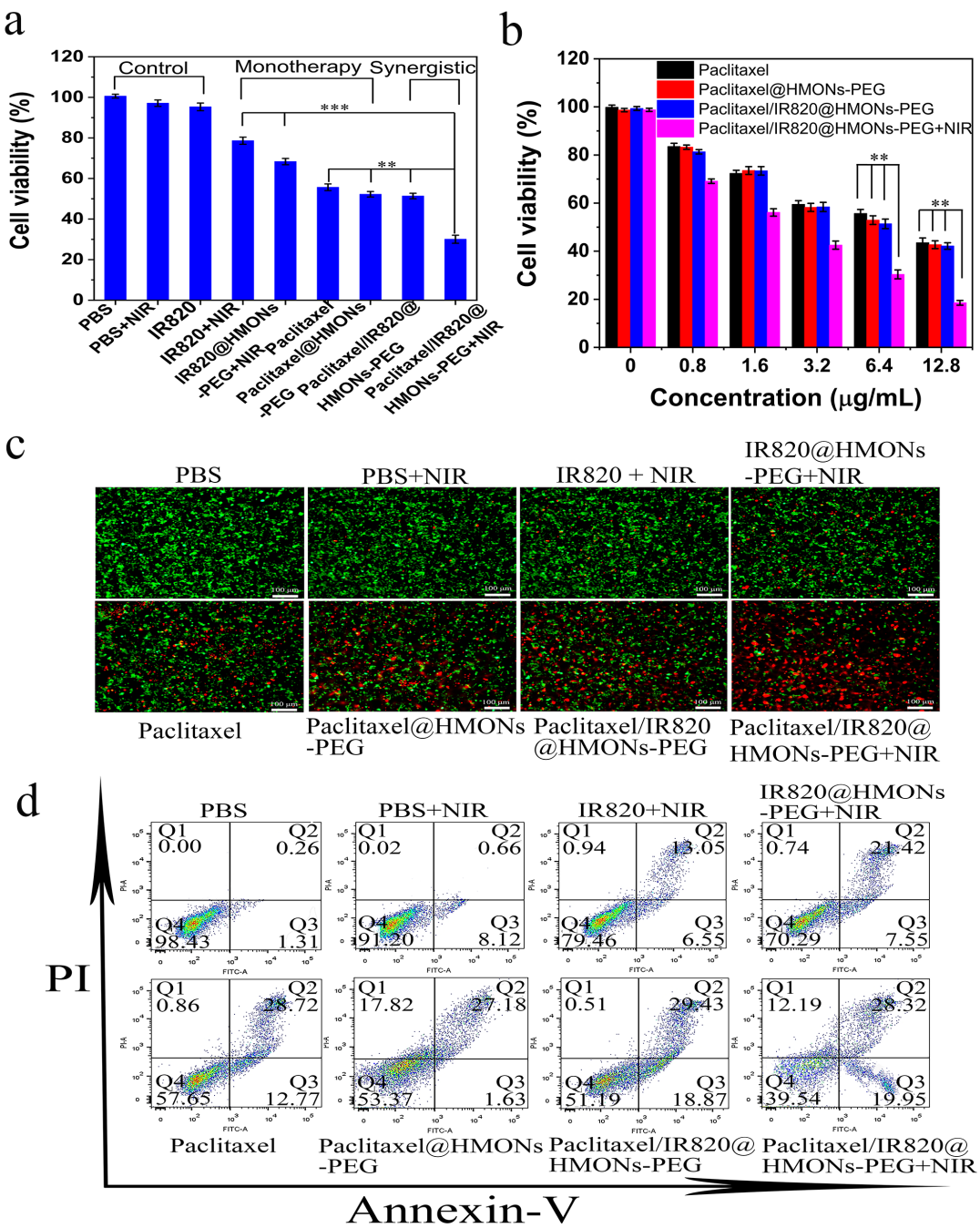

Figure 5.(a)Relative 4T1cell viabilities after incubated with different nanoformulations (b)*In vitro* cell viabilities of Paclitaxel-loaded nanoparticles at different concentrations (c) Calcein-AM/PI staining images of 4T1 cells after different treatments. Scale bar: 100 μm.(d) Flow cytometry analysis for AnnexinV-FITC/PI co-stained 4T1 cells after receiving different treatments with or without laser irradiation for 12 h.

3.7 *In vivo* biodistribution

In vivo fluorescence imaging system was employed for analyzing the tumor-bearing mice's biodistribution and accumulation of Paclitaxel/IR820@HMONs-PEG (10 mg/ kg of IR820) nanoparticles. After 2 h intravenous injection, the fluorescence signals are observed through the mice body (Figure 6a). Then, the fluorescence gradually increases,

with the strongest intensity appearing at the tumor site after 8 h, and maintain until 24 h after treatment. The enhanced permeability and retention (EPR) effect is considered to be the origin of the high tumor accumulation of as-prepared nanoparticles[52]. While fluorescence intensities quickly drop with mice treated with free IR820, which might be attributed to its *in vivo* fast metabolism. Tumors and major organs are collected from the euthanized mice for *ex vivo* fluorescence imaging after 24 h. Mice treated with Paclitaxel/IR820@HMONs-PEG still show strong IR820 fluorescence at the tumor sites after treatment. The fluorescence signals are also found in the livers and kidneys (Figure 6b-c), which may be derived from the metabolism and excretion of the nanoparticles over time[53]. The fluorescence intensity of IR820 is also quantified, which agrees with *ex vivo* fluorescence imaging (Figure 6d). It suggested that Paclitaxel/IR820@HMONs-PEG could prolong retention in the bloodstream and enhanced tumor uptake by the EPR effect.

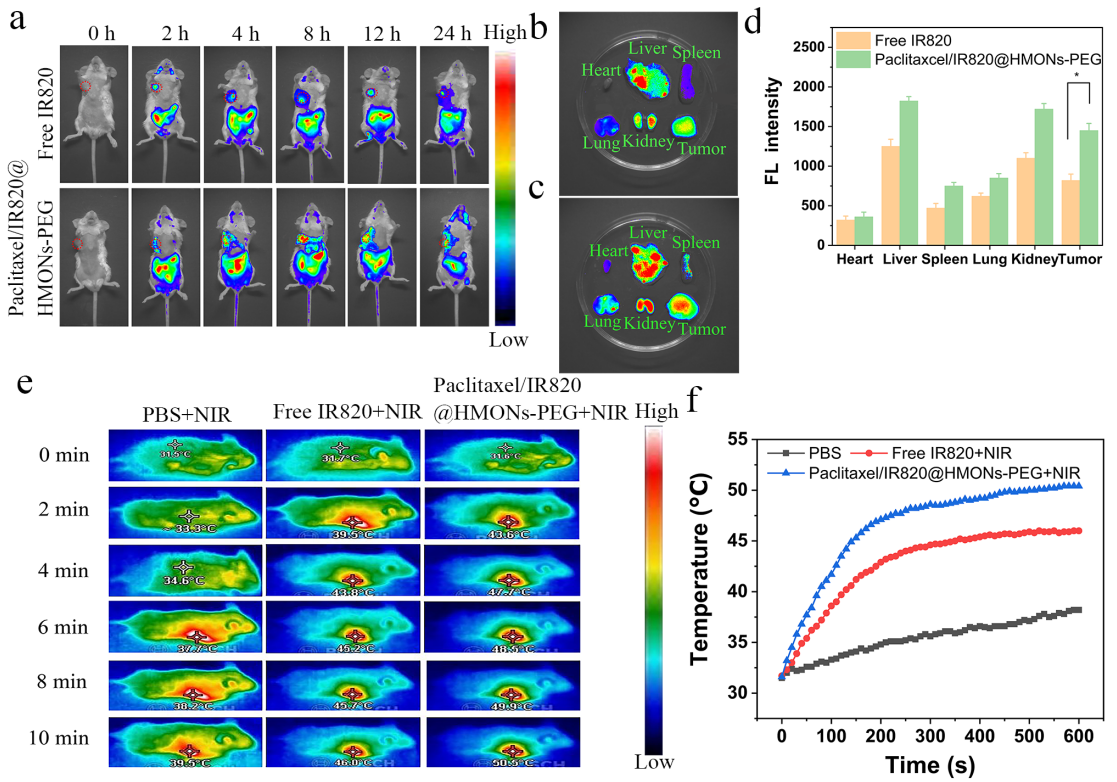

Figure 6.(a) *In vivo* fluorescence of mice after treated with free IR820 or Paclitaxel/IR820@HMONs-PEG nanoparticles at different time points (ellipses denoted the tumor regions). *Ex vivo* fluorescence images of tumors and major organs of mice after treated with (b)free IR820 and (c)Paclitaxel/IR820@HMONs-PEG. (d)Corresponding fluorescence intensities of tumors and major organs after treatment. (e) *In vivo* photothermal images under 808 nm laser irradiation at different time intervals. (f) Temperature change curves of tumors monitored by the infrared thermal camera during laser irradiation.

3.8 Tumor inhibition efficiency *in vivo*

The antitumor effects of chemo-photothermal strategy on 4 T1 tumor-bearing mice was also investigated. As shown in Figure 6e-f, with mice receiving Paclitaxel/IR820@HMONs-PEG+NIR treatment, the tumor temperature increase to 50.6 ℃. At the same time, the PBS treated mice show a negligible increase (< 4 ℃) after NIR treatment, confirming the better photothermal performance of Paclitaxel/IR820@HMONs-PEG. The volume of tumor sharply increase under treatment with PBS+NIR. And for mice treated with paclitaxel, Paclitaxel@HMONs-PEG, and Paclitaxel/IR820@HMONs-PEG without laser irradiation, tumor growth is partially suppressed due to the chemotherapeutic properties of paclitaxel. However, the tumor volumes show only a slight reduction when the mice received free IR820 or IR820@HMONs-PEG plus laser irradiation, resulting from the decreased tumor accumulation of free IR820 and limited therapeutic effect of mono-photothermal therapy (Figure 7a).

On the other hand, the tumor growth is significantly inhibited in Paclitaxel/IR820 @HMONs-PEG under laser irradiation without recurrence throughout treatment, suggesting that the fabricated Paclitaxel/IR820@HMONs-PEG possesses efficient synergistic antitumor efficacy. The mice administered with free paclitaxel show a noticeable weight loss, resulting from the systematic toxicity of paclitaxel[54]. Whereas, no distinct weight loss is observed in other groups, indicating that as-prepared nanocomposites have good biocompatibility (Figure 7b). As displayed in Figure 7c, Paclitaxel@HMONs-PEG group shows reduced tumor weight in comparison with free paclitaxel, which was ascribed to the typical EPR effects. These results are validated by photographs of excised tumors under different treatments (Figure 7d).

To further investigate the combinational therapeutic efficacy, tumors are stained using H&E and TUNEL for histopathology assessments. It is obvious that significant apoptosis/necrosis appear at tumors sites with mice receiving chemo-photothermal synergistic treatment compared with other groups. Besides, the largest area of apoptosis (stained green) is also observed at tumor sections from Paclitaxel/IR820@HMONs-PEG+NIR group by TUNEL analysis (Figure 7e), demonstrating that the constructed nanocomposites have great chemo-phototherapy antitumor effects.

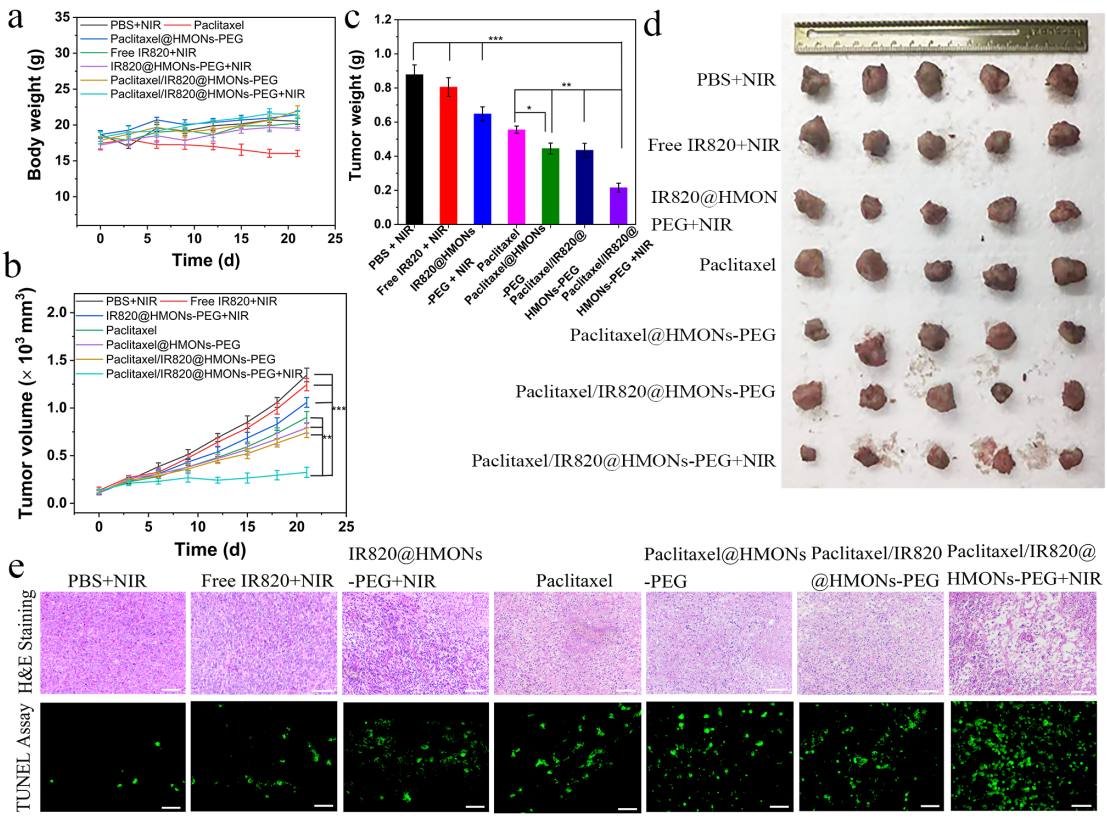

Figure 7. *In vivo* synergistic anticancer therapy of fabricated nanoparticles.(a) Body weight changes and (b)tumor growth curves of tumor-bearing mice after treatment. (c) Tumor weights of mice after 21day treatment from different groups. (d) Photographs of excised tumor tissues after treatment.(e) Images of H&E and TUNELstained tumor slices under different treatments(Scale bar: 50 μm).

3.9 *In vivo* biosafety evaluation

Finally, the histological and hematological analysis were performed to analyze the biocompatibility of the nanoparticles. Negligible side effects could be detected, including inflammation or lesions in heart, liver, spleen, lung, kidney through 21-day treatment (Figure S3). As expected, no significant abnormity of the blood routine and blood chemistry evaluation indexes is found in the treatment groups, confirming the biosafety of the as-prepared nanoplatform (Figure S4).

4. Conclusions

In summary, a unique interface engineered, paclitaxel and IR820 co-delivery nanosystem based on biodegradable HMONs have been successfully developed for combinational chemo-photothermal antitumor therapy. The as-prepared Paclitaxel/ IR820@HMONs-PEG nanosystem exhibits high loading capacity, enhanced biodegradability, improved biocompatibility, controlled drug release and reduced systemic toxicity. Furthermore, the nanosystem possesses excellent photothermal

properties and great photothermal stability, which can efficiently improve cellular uptake and achieve satisfying combinational antitumor therapy. The as-proposed nanosystem holds considerable promise in intelligent drug delivery and synergistic chemo-phototherapy of tumor.

ASSOCIATED CONTENT

Supporting information

EDX spectrum of HMONs; hydrodynamic size of Paclitaxel/IR820@HMONs-PEG dispersed in different medium; H&E images of major organs; blood biochemistry and hematology data.

AUTHOR INFORMATION

Corresponding Authors

Zhaohui Wang - School of Pharmacy, Lanzhou University, 199 Donggang Western Road Lanzhou 730000, People′s Republic of China. E-mail: wangzhaohui@lzu.edu.cn. Tel: +86-931-8915685, Fax: +86-931-8915686.

Yanbin Shi - School of Pharmacy, Lanzhou University, 199 Donggang Western Road Lanzhou 730000, People′s Republic of China. E-mail: shiyb@lzu.edu.cn. Tel: +86-931-8915685, Fax: +86-931-8915686.

Authors

Chunxi Qian - School of Pharmacy, Lanzhou University, 199 Donggang Western Road Lanzhou 730000, People′s Republic of China.

Bandar Al-Hamyari - School of Pharmacy, Lanzhou University, 199 Donggang Western Road Lanzhou 730000, People′s Republic of China.

Xiaofei Tang - School of Pharmacy, Lanzhou University, 199 Donggang Western Road Lanzhou 730000, People′s Republic of China.

Bo Hou - School of Physics and Astronomy, Cardiff University, Cardiff, Wales, CF24 3AA, United Kingdom.

Shuaibo Yang - School of Pharmacy, Lanzhou University, 199 Donggang Western

Road Lanzhou 730000, People′s Republic of China.
Guifang Zhang - School of Pharmacy, Lanzhou University, 199 Donggang Western Road Lanzhou 730000, People′s Republic of China.
Huijuan Lv - School of Pharmacy, Lanzhou University, 199 Donggang Western Road Lanzhou 730000, People′s Republic of China.
Zhigang Yang - School of Pharmacy, Lanzhou University, 199 Donggang Western Road Lanzhou 730000, People′s Republic of China.

Author contributions

Chunxi Qian: Investigation, Methodology, Writing - original draft, Data curation. Bandar Al-Hamyari: Formal analysis, Data curation. Xiaofei Tang: Investigation, Data curation, Resources. Bo Hou: Writing-review & editing. Shuaibo Yang: Conceptualization, Formal analysis. Guifang Zhang: Methodology, Data curation. Huijuan Lv: Investigation, Data curation. Zhigang Yang: Conceptualization, Resources. Zhaohui Wang: Funding acquisition, Resources. Yanbin Shi: Supervision, Validation, Funding acquisition, Writing-review & editing.

Notes

The authors declare that there are no conflicts of interest for this work.

Acknowledgements

This work was financially supported by Key Natural Science Foundation of Gansu province (20JR10RA585).

References

1 Sung, H.; Ferlay, J.; Siegel, R. L.; Laversanne, M.; Soerjomataram, I.; Jemal, A.; Bray, F. Global Cancer Statistics 2020: GLOBOCAN Estimates of Incidence and Mortality Worldwide for 36 Cancers in 185 Countries. *CA Cancer J. Clin.* 2021, 71, 209-249.

2 Tang, Y.; Lei, T.; Manchanda, R.; Nagesetti, A.; Fernandez-Fernandez, A.; Srinivasan, S.; McGoron, A. J. Simultaneous delivery of chemotherapeutic and thermal-optical agents to cancer cells by a

polymeric (PLGA) nanocarrier: an in vitro study. *Pharm. Res.* 2010, 27, 2242-2253.

3 Wong, P.-T.; Choi, S. K. Mechanisms of drug release in nanotherapeutic delivery systems. *Chem. Rev.* 2015, 115, 3388-3432.

4 Hu, Q.-Y.; Sun, W.-J.; Wang, C.; Gu, Z. Recent advances of cocktail chemotherapy by combination drug delivery systems. *Adv. Drug Deliv. Rev.* 2016, 98, 19-34.

5 Karimi, M.; Ghasemi, A.; Zangabad, P. S.; Rahighi, R.; Basri, S. M.; Mirshekari, H.; Amiri, M.; Shafaei Pishabad, Z.; Aslani, A.; Bozorgomid, M.; Ghosh, D.; Beyzavi, A.; Vaseghi, A.; Aref, A. R.; Haghani, L.; Bahrami, S.; Hamblin, M. R. Smart micro/nanoparticles in stimulus-responsive drug/gene delivery systems. *Chem. Soc. Rev.* 2016, 45, 1457-1501.

6 Xu, S.; Olenyuk, B. Z.; Okamoto, C. T.; Hamm-Alvarez, S. F. Targeting receptor-mediated endocytotic pathways with nanoparticles: rationale and advances. *Adv. Drug Deliv. Rev.* 2013, 65,121-138.

7 Wang, Y.; Song, S.; Zhang, S.; Zhang, H. Stimuli-Responsive Nanotheranostics Based on Lanthanide-Doped Upconversion Nanoparticles for Cancer Imaging and Therapy: Current Advances and Future Challenges. *Nano Today*. 2019, 25, 38-67.

8 Wang, Z.; Ju, Y.; Ali, Z.; Yin, H.; Sheng, F.; Lin, J.; Wang, B.; Hou, Y. Near-Infrared Light and Tumor Microenvironment Dual Responsive Size-Switchable Nanocapsules for Multimodal Tumor Theranostics. *Nat. Commun.* 2019, 10, 4418.

9 Meng, Z.; Zhou, X.; She, J.; Zhang, Y.; Feng, L.; Liu, Z. Ultrasound-Responsive Conversion of Microbubbles to Nanoparticles to Enable Background-Free in Vivo Photoacoustic Imaging. *Nano Lett.* 2019, 19, 8109-8117.

10 Zhang, P.; Wang, J.; Chen, H.; Zhao, L.; Chen, B.; Chu, C.; Liu, H.; Qin, Z.; Liu, J.; Tan, Y.; Chen, X.; Liu, G. Tumor Microenvironment-Responsive Ultrasmall Nanodrug Generators with Enhanced Tumor Delivery and Penetration. *J. Am. Chem. Soc.* 2018, 140, 14980-14989.

11 Sun, H.; Zhang, Y.; Chen, S.; Wang, R.; Chen, Q.; Li, J.; Luo, Y.; Wang, X.; Chen, H. Photothermal Fenton Nanocatalysts for Synergetic Cancer Therapy in the Second Near-Infrared Window. *ACS Appl. Mater. Interfaces.* 2020, 12, 30145–30154.

12 Xin, J.-Y.; Zhang, K.; Huang, J.-Q.; Luo, X.-J.; Gong, X.-Q.; Yang, Z.-X.; Lin, H.-Y.; Shan, H.; Gao, J.-H. Facile synthesis of aquo-cisplatin arsenite multidrug nanocomposites for overcoming drug resistance and efficient combination therapy. *Biomater. Sci.* 2019, 7, 262-271.

13 Li, D.-J.; Zhang, T.; Min, C.-W.; Huang, H.; Tan, D. H.; Gu, W. G.; Biodegradable theranostic nanoplatforms of albumin-biomineralized nanocomposites modified hollow mesoporous organosilica for photoacoustic imaging guided tumor synergistic therapy. *Chem. Eng. J. 2*020, 388, 124253.

14 Hu, T.; Yan, L.; Wang, Z.; Shen, W.; Liang, R.; Yan, D.; Wei, M. A pH-responsive ultrathin Cu-based nanoplatform for specific photothermal and chemodynamic synergistic therapy. *Chem. Sci.* 2021, 12, 2594-2603.

15 Wang, F.; Hu, Chuan.; Zhou, Y.; Gao, H.-L.; Hu, J. The progress and perspective of nanoparticle-enabled tumor metastasis treatment. Acta Pharm Sin B. 2020, 10, 2037-2053.

16 Wu, B.-Y.; Fu, J.-T.; Zhou, Y.-X.; Luo, S.-L.; Zhao, Y.-T.; Quan, G.-L.; Pan, X.; Wu, C.-B. Tailored core-shell dual metal-organic frameworks as a versatile nanomotor for effective synergistic antitumor therapy. Acta Pharm Sin B. 2020, 10, 2198-2211.

17 Yu, W.-Q.; Shevtsov, Maxim.; Yu, W.-Q.; Chen, X.-C.; Gao, H.-L. Advances in aggregatable nanoparticles for tumor-targeted drug delivery. Chin Chem Lett. 2020, 31, 1366-1374.

18 Chen, B.; Mei, L.; Fan, R.-R.; Wang, Y. L.; Nie, C.-L.; Tong, A. P.; Guo, G. Facile construction of targeted pH-responsive DNA-conjugated gold nanoparticles for synergistic photothermal-chemotherapy. Chin Chem Lett. 2021, 32, 1775-1779.

19 Fan, W.-P.; Yung, B.; Huang, P.; Chen, X.-Y. Nanotechnology for Multimodal Synergistic Cancer Therapy. *Chem. Rev.* 2017, 117, 13566-13638.

20 He, T.; He, J.; Younis, M. R.; Blum, N. T.; Lei, S.; Zhang, Y.-l.; Huang, P.; Lin, J. Dual-Stimuli-Responsive Nanotheranostics for Dual-Targeting Photothermal-Enhanced Chemotherapy of Tumor. *ACS Appl. Mater. Interfaces.* 2021, 13, 22204-22212.

21 Hu, X.; Tian, H.-L.; Jiang, W.; Song, A.-X.; Li, Z.-H.; Luan, Y.-X. Rational Design of IR820 and Ce6-Based Versatile Micelle for Single NIR Laser–Induced Imaging and Dual-Modal Phototherapy. *Small*. 2018, 14, 1802994.

22 Liu, B.; Li, C.-X.; Chen, G.-Y.; Liu, B.; Deng, X.-R.; Wei, Y.; Xia, J.; Xing, B.-G.; Ma, P.-A.; Lin, J. Synthesis and Optimization of MoS2@Fe3O4-ICG/Pt(IV) Nanoflowers for MR/IR/PA Bioimaging and Combined PTT/PDT/Chemotherapy Triggered by 808 nm Laser. *Adv. Sci.* 2017, 4, 1600540.

23 Li, W.; Peng, J.; Tan, L.; Wu, J.; Shi, K.; Qu, Y.; Wei, X.; Qian, Z. Mild photothermal

therapy/photodynamic therapy/chemotherapy of breast cancer by Lyp-1 modified Docetaxel/IR820 Co-loaded micelles. *Biomaterials*. 2016, 106, 119-133.

24 Liu, Y.-J.; Bhattarai, P.; Dai, Z.-F.; Chen, X.-Y. Photothermal therapy and photoacoustic imaging via nanotheranostics in fighting cancer. *Chem. Soc. Rev.* 2019, 48, 2053-2108.

25 Chen, W.-S.; Ouyang, J.; Liu, H.; Chen, M.; Zeng, K.; Sheng, J.-P.; Liu, Z.-J.; Han, Y.-J.; Wang, L.-Q.; Li, J.; Deng, L.; Liu, Y.-N.; Guo, S.-J. Black phosphorus nanosheet-based drug delivery system for synergistic photodynamic / photothermal /chemotherapy of cancer. *Adv. Mater.* 2017, 29, 1603864.

26 Girma, W.-M.; Tzing, S.-H.; Tseng, P.-J.; Huang, C.-C.; Ling, Y.-C.; Chang, J.-Y. Synthesis of Cisplatin(IV) prodrug-tethered CuFeS2 nanoparticles in tumor-targeted chemotherapy and photothermal therapy. *ACS Appl. Mater. Interfaces.* 2018, 10, 4590-4602.

27 Chen, Y.; Meng, Q.-S.; Wu, M.-Y.; Wang, S.-G.; Xu, P.-F.; Chen, H.-R.; Li, Y.-P.; Zhang, L.-X.; Wang, L.-Z.; Shi, J.-L. Hollow mesoporous organosilica nanoparticles: a generic intelligent framework-hybridization approach for biomedicine. *J. Am. Chem. Soc.* 2014, 136, 16326-16334.

28 Teng, Z.-G.; Li, W.; Tang, Y.-X.; Elzatahry, A.; Lu, G.-M.; Zhao, D.-Y. Mesoporous Organosilica Hollow Nanoparticles: Synthesis and Applications. *Adv. Mater.* 2019, 31, 1707612.

29 Fang, X.-L.; Zhao, X. J.; Fang, W. J.; Chen, C.; Zheng, N.-F. Self-templating synthesis of hollow mesoporous silica and their applications in catalysis and drug delivery. *Nanoscale*. 2013, 5, 2205-2218.

30 Du, X.; Kleitz, F.; Li, X.-Y.; Huang, H.-W.; Zhang, X.-J.; Qiao, S.-Z. Disulfide-Bridged Organosilica Frameworks: Designed, Synthesis, Redox-Triggered Biodegradation, and Nanobiomedical Applications. *Adv. Funct. Mater.* 2018, 28, 1707325.

31 Huang, P.; Chen, Y.; Lin, H.; Yu, L.; Zhang, L.; Wang, L.; Zhu, Y.; Shi, J. Molecularly organic/inorganic hybrid hollow mesoporous organosilica nanocapsules with tumor-specific biodegradability and enhanced chemotherapeutic functionality. *Biomaterials*. 2017, 125, 23-37.

32 Huang, P.; Qian, X.-Q.; Chen, Y.; Yu, L.-D.; Lin, H.; Wane, L. Y.; Zhu, Y.-F.; Shi, J.-L. Metalloporphyrin encapsulated biodegradable nanosystems for highly efficient magnetic resonance imaging-guided sonodynamic cancer therapy. *J. Am. Chem. Soc.* 2017, 139, 1275-1284.

33 Lu, N.; Fan, W.-P.; Yi, X.; Wang, S.; Wang, Z.-T.; Tian, R.; Jacobson, O.; Liu, Y.-J.; Yung, B. C.; Zhang, G.-F.; Teng, Z.-G.; Yang, K.; Zhang, M.-M.; Niu, G.; Lu, G.-M.; Chen, X.-Y. Biodegradable

hollow mesoporous organosilica nanotheranostics for mild hyperthermia-induced bubble-enhanced oxygen-sensitized radiotherapy. *ACS Nano.* 2018, 12, 1580-1591.

34 Zhang, J.-J.; Lu, N.; Weng, L.-X.; Feng, Z.-H.; Tao, J.; Su, X.-D.; Yu, R.-F.; Shi, W.-H.; Qiu, Q.; Teng, Z.-G.; Wang, L.-H. General and facile syntheses of hybridized deformable hollow mesoporous organosilica nanocapsules for drug delivery. *J. Colloid Interface Sci.* 2021, 583, 714-721.

35 Weon, C. C.; Suep, B. J.; Heon, K. J.; Sook, P. J. Modification of paclitaxel-loaded solid lipid nanoparticles with 2-hydroxypropyl-β-cyclodextrin enhances absorption and reduces nephrotoxicity associated with intravenous injection. *Int. J. Nanomedicine.* 2015, 10, 5397-5405.

36 Najlah, M.; Kadam, A.; Wan, K.-W.; Ahmed, W.; Taylor, K. M. G.; Elhissi, A. M. A. Novel paclitaxel formulations solubilized by parenteral nutrition nanoemulsions for application against glioma cell lines. *Int. J. Pharm.* 2016, 506, 102-109.

37 Utreja, P.; Jain, S.; Tiwary, A. K. Localized delivery of paclitaxel using elastic liposomes: Formulation development and evaluation. *Drug Deliv.* 2011, 18, 367-376.

38 Chen, L.-N.; Chen, B.-C.; Deng, L.; Gao, B.-A.; Zhang, Y.-S.; Wu, C.; Yu, N.; Zhou, Q.-Q.; Yao, J.-Z.; Chen, J.-M. An optimized two-vial formulation lipid nanoemulsion of paclitaxel for targeted delivery to tumor. *Int. J. Pharm.* 2017, 534, 308-315.

39 Yang, X.-Y.; Cai, X.-Q.; Yu, A.-H.; Xi, Y.-W.; Zhai, G.-X. Redox-sensitive self-assembled nanoparticles based on alpha-tocopherol succinate-modified heparin for intracellular delivery of paclitaxel. *J. Colloid Interface Sci.* 2017, 496, 311-326.

40 Chang, J.-E.; Cho, H. J.; Yi, E.-J.; Kim, D. D.; Jheon, S. h. Hypocrellin B and paclitaxel-encapsulated hyaluronic acid–ceramide nanoparticles for targeted photodynamic therapy in lung cancer. *J. Photoch.Photobio.B.* 2016, 158, 113-121.

41 Wu, J.-R.; Williams, G. R.; Niu, S.-W.; Gao, F.; Tang, R.-R.; Zhu, L.-M. A Multifunctional Biodegradable Nanocomposite for Cancer Theranostics. *Adv. Sci.* 2019, 6, 1802001.

42 Wang, X.-W.; Zhong, X.-Y.; Lei, H.-L.; Geng, Y.-H.; Zhao, Q.; Gong, F., Yang, Z.-J.; Dong, Z.-L.; Liu, Zhuang.; Cheng, L. Hollow Cu2Se Nanozymes for Tumor Photothermal-Catalytic Therapy. Chem. Matter. 2019, 31, 6174-6186.

43 Liu, J.; Yang, Q.; Zhang, L.; Jiang, D.; Shi, X.; Yang, J.; Zhong, H.; Li, C. Thioether-bridged Mesoporous Organosilicas: Mesophase Transformations Induced by the Bridged Organosilane

Precursor. *Adv. Funct. Mater.* 2007, 17, 569-576.

44 Wu, M.-Y.; Meng, Q.-S.; Chen, Y.; Du, Y.-Y.; Zhang, L.-X.; Li, Y.-P.; Zhang, L.-L.; Shi, J.-L. Large-Pore Ultrasmall Mesoporous Organosilica Nanoparticles: Micelle/ Precursor Co-templating Assembly and Nuclear-Targeted Gene Delivery. *Adv. Mater.* 2015, 27, 215-222.

45 Yu, L.-D.; Chen, Y.; Lin, H.; Du, W.-X.; Chen, H.-R.; Shi, J.-l. Ultrasmall meso-porous organosilica nanoparticles: Morphology modulations and redox-responsive biodegradability for tumor-specific drug delivery. *Biomaterials*. 2018, 161, 292-305.

46 Lee, M. H.; Yang, Z.-G.; Lim, C. W.; Lee, Y. H.; Bang, S.-D.; Kang, C.-H.; Kim, J. S. Disulfide-Cleavage-Triggered Chemosensors and Their Biological Applications. *Chem. Rev.* 2013, 113, 5071-5109.

47 Chen, B.-L.; Dai, W.-B.; He, B.; Zhang, H.; Wang, X.-Q.; Wang, Y.-G.; Zhang, Q. Current Multistage Drug Delivery Systems Based on the Tumor Microenvironment. *Theranostics.* 2017, 7, 538-558.

48 Li, Y.-P.; An, L.; Lin, J.-M.; Tian, Q.-W.; Yang, S.-P. Smart nanomedicine agents for cancer, triggered by pH, glutathione, H_2O_2, or H_2S. *Int. J. Nanomedicine.* 2019, 14, 5729-5749.

49 Chen, Y.; Xu, P.-F.; Chen, H.-R.; Li, Y.-S.; Bu, W.- B.; Shu, Z.; Li, Y.-P.; Zhang, J.-M.; Zhang, L.-X.; Pan, L.-M.; Cui, X.-Z.; Hua, Z.-L.; Wang, J.; Zhang, L.-L.; Shi, J.-L. Colloidal HPMOs NPs: Silica-Etching Chemistry Tailoring, Topological Transformation and Nano-Biomedical Applications. *Adv. Mater.* 2013, 25, 3100–3105.

50 Goodman, A. M.; Neumann, O.; Norregaard, K.; Henderson, L.; Choi, M. R.; Clare, S. E.; Halas, N. J. Near-infrared remotely triggered drug-release strategies for cancer treatment. *Proc. Natl. Acad. Sci. U. S. A.* 2017, 114, 12419-12424.

51 Sun, X.; Zhang, G.; Keynton, R. S.; O'Toole, M. G.; Patel, D.; Gobin, A. M. Enhanced drug delivery via hyperthermal membrane disruption using targeted gold nanoparticles with PEGylated Protein-G as a cofactor. *Nanomed. Nanotechnol.* 2013, 9, 1214-1222.

52 Huang, X.; Zhang, W.; Guan, G.; Song, G.; Zou, R.; Hu, J. Design and Functionalization of the NIR-Responsive Photothermal Semiconductor Nanomaterials for Cancer Theranostics. *Acc. Chem. Res.* 2017, 50, 2529-2538.

53 Xuan, M.; Shao, J.; Zhao, J.; Li, Q.; Dai, L.; Li, J. Magnetic Mesoporous Silica Nanoparticles Cloaked by Red Blood Cell Membranes: Applications in Cancer Therapy. *Angew. Chem. Int. Ed.*

2018, 57, 6049-6053.

54 Cao, J.-Y.; Wang, R.; Gao, N.; Li, M.-H.; Tian, X.-Y.; Yang, W.-L.; Ruan, Y.; Zhou, C.-L; Wang, G.-T.; Liu, X.-Y.; Tang, S.- K.; Yu, Y.; Liu, Y.; Sun, G.-Y.; Peng, H.-S.; Wang, Q. A7RC peptide modified paclitaxel liposomes dually target breast cancer. *Biomater. Sci.* 2015, 3, 1545-1554.